

# ***Ab initio* calculation of the solution enthalpies of substitutional and interstitial impurities in paramagnetic fcc Fe**

A. V. Ponomareva,<sup>1</sup> Yu. N. Gornostyrev,<sup>2,3</sup> and I. A. Abrikosov<sup>4</sup>

<sup>1</sup>*Materials Modeling and Development Laboratory, National University of Science and Technology "MISIS", Moscow, Russia, 119049*

<sup>2</sup>*Institute of Quantum Materials Science, Ekaterinburg, Russia, 620075*

<sup>3</sup>*Institute of Metal Physics, Ural Branch of the Russian Academy of Sciences, Ekaterinburg, Russia, 620219*

<sup>4</sup>*Department of Physics, Chemistry, and Biology (IFM), Linköping University, Linköping, Sweden, SE-581 83*

(Received 15 March 2014; revised manuscript received 28 June 2014; published 30 July 2014)

In the framework of disordered local moment approach by using magnetic sampling method, we suggested a model that takes into account the magnetic disorder in paramagnetic Fe with point defects. We calculate solution enthalpies of substitutional (Nb, V) and interstitial (C, N) impurities in paramagnetic face-centered cubic Fe and obtain results that are in agreement with available experimental data. It is found that both interstitial and substitutional atoms may favor the local magnetic polarization of the Fe host around the impurities by decreasing the potential energy of the system. The possibility of a formation of predominantly ferromagnetic Fe clusters around carbon in the temperature range of overcooled austenite is discussed.

DOI: [10.1103/PhysRevB.90.014439](https://doi.org/10.1103/PhysRevB.90.014439)

PACS number(s): 75.20.En, 71.20.Be, 71.70.Gm

## **I. INTRODUCTION**

Theoretical methods based on density functional theory (DFT) give solid ground to predict solution enthalpies  $H_{\text{sol}}$  of impurities from first principles for nonmagnetic and magnetically ordered materials. At the same time, calculations for point defects in paramagnetic hosts, like in Fe above the magnetic ordering temperature, are quite challenging for the theory. Because of the existence of local magnetic moments above the magnetic transition temperature in the itinerant magnets [1], one deals with a many-electron problem whose solution goes beyond the standard DFT implementations. In principle, one could use the dynamical mean-field theory (DMFT) [2], combined with local or semilocal DFT band structure calculations. It has been used in papers on finite-temperature magnetism in body-centered cubic (bcc) [3,4] and face-centered cubic (fcc) Fe [5], as well as structural Fe [6] and electronic [7] phase transition in this metal. However, reducing symmetry of a system by introducing defects makes DMFT calculations quite time consuming. A successful approach that has become quite popular in practical applications is given by the so-called disordered local moment (DLM) model, introduced by Hubbard [8] and Hasegawa [9] and combined with the local spin density approximation DFT by Gyorffy *et al.* [10]. Within DLM, the magnetically disordered state is described as a pseudoalloy of equal amounts of atoms with spin-up and spin-down orientations of their magnetic moments. However, until recently, the DLM was used exclusively in the framework of the coherent potential approximation (CPA) [10]. This made it unsuitable in papers on defects that induce large local distortions of the crystal lattice, such as interstitial impurities. A formal generalization of the DLM approach towards the supercell techniques has been presented recently by Alling *et al.* [11], where the method has been successfully applied for simulations of CrN compound. Here, we extend the technique towards applications for solids with defects.

The impurities and alloying elements play a decisive role in the microstructure formation, and they have strong influence on many key properties of, e.g., steels. In particular, a precipitation of carbides and nitrides of V and Nb is an

important tool in tailoring the low-alloyed steels for pipe and ship applications [12]. The formation of these particles increases strength and prevents the austenite grain growth during hot rolling. Thus, understanding of thermodynamic and kinetic of the carbide/nitride precipitation is highly important for an optimization of technological schemes and improvement of the steel properties [13]. Solubility of the carbides and nitrides is usually expressed as a product of solubility limits of their components by an empiric relation  $\ln(C_{Me}C_X) = A - B/T$  [13], where  $Me = \text{Nb, V}$ ;  $X = \text{C, N}$ ; and  $B$  is determined by formation energies of carbides or nitrides and solubility enthalpies of their components. In principal, these values can be deduced from computational thermodynamic (CALPHAD) approach, which uses the sophisticated interpolation of experimental data. Unfortunately, the reliability of the description is restricted by a huge dispersion of experimental values of solubility [13] that originated from the mutual effect of C, N, or other alloying elements on carbonitride thermodynamics. Recently, the solubility product of NbC in ferromagnetic (FM) bcc Fe has been computed from DFT [14]. At the same time, the technologically important temperature of, e.g., NbC precipitation corresponds to the austenite region, i.e., to the paramagnetic fcc Fe.

It is known [15] that the solubility of interstitial impurities (C, N) in the fcc Fe is much higher than in the bcc phase (ferrite). This is so because the stronger lattice distortions near the impurity result in the higher solution energies for the bcc Fe. However, changes due to the impurities in electronic and magnetic properties may be also important [16]. Moreover, the strain energy is much smaller for substitutional atoms (especially for V), and electronic contribution should dominate the solution enthalpy. As a result, one can expect that the presence of the substitutional impurities will also influence the magnetic state of iron.

However, there have been only a few attempts to calculate  $H_{\text{sol}}$  of C in fcc Fe [14,16,17]. The situation is complicated by the magnetic ground state being described incorrectly by the DFT calculations in the local or semilocal approximation. At low temperature, the spin spiral states have been observed experimentally in  $\gamma$ -iron from the precipitates of fcc Fe in

Cu matrix [18,19], which has been only partly confirmed by first-principles noncollinear calculations [20–23]. The  $\gamma$  phase of iron is stable at temperatures above the magnetic order-disorder transition, where thermal fluctuations can be very strong. In Ref. [17], the DFT calculations were performed for dissolution and diffusion of carbon in iron. For  $\gamma$ -Fe, which was modeled as a FM high-spin phase,  $H_{\text{sol}} = -0.17$  eV. This indicated that the dissolution of carbon in fcc Fe should be exothermic. On the other hand, the experimental value is about 0.4 eV [24]. It was also shown in Ref. [17] that the calculated value of the diffusion barrier for carbon in nonmagnetic fcc Fe (2.7 eV) was quite different from the experimental value (1.59 eV [25]), underlining that the nonmagnetic state is not suitable for a description of austenite. Magnetic structure and local perturbations near carbon impurity in  $\gamma$ -iron were investigated by *ab initio* electronic structure calculations in Ref. [16], where the authors found that  $H_{\text{sol}}$  is  $\sim 0.55$  eV in the double antiferromagnetic state. The authors concluded that in  $\gamma$ -iron, there is the complex magnetic structure with strong tetragonal distortions and a strong tendency to formation of local FM clusters near carbon impurities. This result highlights the important role of magnetism in thermodynamics of Fe-based alloys (see Refs. [26,27]).

In this paper, the results of calculations of solution enthalpies of substitutional (Nb, V) and interstitial (C, N) impurities in paramagnetic  $\gamma$ -Fe are presented. In the framework of the DLM approach and by using the magnetic sampling method (MSM) [11] we introduce a model that allow us to account for the magnetic disorder in the system and investigate its effect on impurity dissolution enthalpy. An influence of impurities on local and global properties of  $\gamma$ -Fe and a possibility to induce magnetic polarization around the impurity in the paramagnetic state in the premartensitic temperature region are discussed.

## II. METHOD

### A. General computational details

We carried out calculations using a supercell technique and an all-electron projector-augmented wave (PAW) method as implemented in the Vienna *Ab initio* Simulation Package (VASP) code [28–30]. C and N atoms were located in octahedral interstitial sites, while V and Nb atoms occupied substitutional positions. Simulations were carried using  $\text{Fe}_{108}$ ,  $\text{Fe}_{107}\text{X}_1$  ( $X = \text{V}, \text{Nb}$ ), and  $\text{Fe}_{108}\text{X}_1$  ( $X = \text{C}, \text{N}$ ) periodic supercells. The generalized gradient approximation (GGA) [31] was used for treating electron exchange-correlation effects. The convergence criterion for the electronic subsystem was chosen to be equal to  $10^{-4}$  eV for two subsequent iterations, and the ionic relaxation loop within the conjugated gradient method was stopped when forces became on the order of  $10^{-3}$  eV/Å. Each supercell considered in this paper is relaxed according to its Hellmann-Feynman forces [32,33]. Brillouin zone sampling was performed using the Methfessel-Paxton smearing method with  $\text{SIGMA} = 0.1$  [34]. The volume and shape of the cell were fixed during the iterations. The energy cutoff for plane waves included in the expansion of wave functions was set to 500 eV. Sampling of the Brillouin zone was done using a Monkhorst-Pack scheme [35] on a grid of

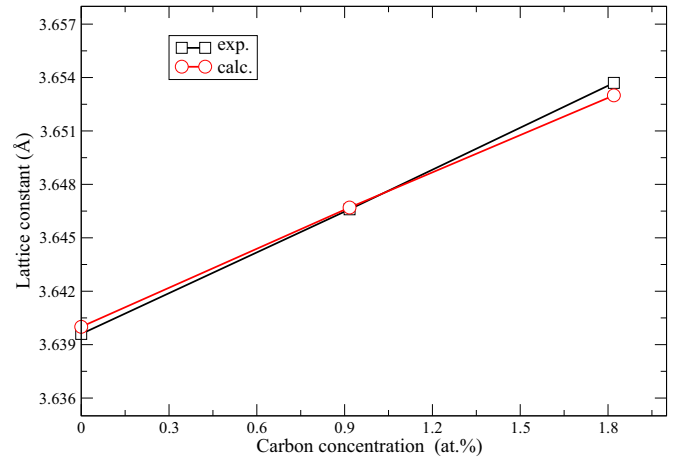


FIG. 1. (Color online) Calculated (calc.) and experimental (exp.) [36,37] ( $T \sim 1100$  K) lattice constants as a function of the carbon content in fcc Fe.

$2 \times 2 \times 2$  k-points. We checked that  $4 \times 4 \times 4$  k-mesh calculations changed values of impurity solution enthalpy by less than 0.002 eV. All electronic structure calculations were carried out at zero electronic and ionic temperatures.

### B. Choice of lattice parameter

At high temperature, effects of thermal expansion and magnetic entropy are important. They are not captured in DFT total energy calculations at  $T = 0$  K. The lattice parameter in this case does not correspond to the total energy minimum. We solve this problem by carrying out simulations at the experimental lattice parameter fixed to its high-temperature value in fcc Fe and at constant zero-temperature pressure corresponding to this lattice parameter. In this case, possible variations of lattice parameter between pure Fe and supercell with an impurity become more important than for  $T = 0$  K calculations, because one cannot rely on variational cancellation of errors present near the total energy minima. In principle, if the supercell is large enough, this should not be a problem. However, computational costs scale as  $N^3$  with the supercell size, and it may become impractical to do calculations at such big supercells.

To check the accuracy of the constant zero-temperature pressure calculations at the experimental lattice parameter, we compared the theoretical and experimental variations of the lattice parameter with increasing carbon fraction. Results are presented in Fig. 1. The experimental data were acquired using neutron diffraction, which seems to be a more suitable technique for determining the lattice parameter of austenite in Fe-C alloys at high temperature due to reduced sensitivity to surface decarburization [36,37]. The lattice parameters of  $\text{Fe}_{108}\text{C}_1$  and  $\text{Fe}_{108}\text{C}_2$  supercells were chosen so that their pressure corresponded to that of the Fe supercell. From Fig. 1, we can see that constant pressure calculations provide the correct value of  $da/dc$ , which justifies the procedure described above and increases the possibility for a good convergence of our results with the size of the supercell.

For practical calculations of the solution enthalpy, we adjusted the lattice constant of pure fcc Fe to equalize the

pressure between Fe and Fe- $X$  periodic cells, while the latter was fixed to experimental lattice parameter of paramagnetic  $\gamma$ -Fe at  $T \sim 1200$  K and  $a = 3.647$  Å [38]. Thus, within our procedure, the zero-temperature pressure was fixed to that of a system with an impurity rather than to that of a pure fcc Fe. This greatly reduced computational costs in comparison to adjusting the lattice constant of Fe- $X$  supercells to equalize their pressure with that of pure Fe. Lattice parameter for the latter turned out to fluctuate slightly around the mean value 3.64 Å. One may wonder whether this computational scheme introduced an additional error. To answer this question, we analyzed how small variations of pressure affected the results of the solution enthalpy calculations. We observed that within the reasonable pressure interval, the effect turned out to be negligible (see the Appendix, particularly Table II).

### C. Simulation of magnetic disorder

Generally, the high-temperature paramagnetic phase cannot be adequately reproduced by a nonmagnetic state [39]. A more adequate description is provided by the DLM model [10] adopted in this paper. Moreover, we go beyond the original implementation of the DLM in the framework of the CPA [10] and, in this paper, simulate the paramagnetic state of pure  $\gamma$ -Fe (without impurities) using the magnetic special quasirandom structure (SQS) technique [40]. We consider  $\text{Fe}_{50}^{\uparrow}\text{Fe}_{50}^{\downarrow}$  alloy as a collinear system with an equal amount of spin-up and spin-down atoms and the spin correlation functions, which are close to zero for the first six coordination shells. Because fcc Fe is thermodynamically stable well above its estimated Neel temperature, the effects of magnetic short-range order should be negligible. It was demonstrated earlier [10] that for a completely uncorrelated magnetic subsystem, the two pictures, collinear and noncollinear, lead to the same thermodynamic descriptions.

The SQS model describes a static picture of the “frozen” magnetic disorder and does not account for the spin dynamics. However, atomic diffusion processes are several orders of magnitude slower than the magnetic degrees of freedom; therefore, on the timescale associated with the diffusion, magnetic fluctuations are almost instant. This means that the impurity will sense many different magnetic configurations rather than only one. The latter would be the case if the magnetic SQS method is used straightforwardly for the description of paramagnetic  $\gamma$ -Fe with the impurity. To catch the dynamic behavior of the magnetic system, we should approximate the paramagnetic material by a set of many magnetic configurations and average the obtained result over them. In Ref. [11], the MSM has been proposed to treat the magnetic disorder and the thermodynamics of paramagnetic materials. In MSM, one creates a large set of supercells with randomly generated magnetic configurations and with a vanishing net magnetic moment. The running average of their energies is taken as the potential energy of the disordered paramagnetic state. The MSM has been applied for the description of the high-temperature paramagnetic CrN (without defects) in Ref. [11]. It was shown that MSM calculations converged already for 40 different magnetic distributions and that the two methods, the MSM and SQS, gave almost identical results [11]. Moreover, the MSM results for thermodynamic

properties of CrN were in good agreement with those obtained in DLM-molecular dynamics simulations by Steneteg *et al.* [41], where the dynamical behavior of a paramagnetic system was treated explicitly.

We base our calculations for  $\gamma$ -Fe with impurities on the idea behind the MSM but combine it with the magnetic SQS method used for pure Fe to allow for an accurate description of small energy differences between the impure and the reference states. The proposed MSM-SQS scheme for the calculation of solution enthalpies is as follows. First, we use the magnetic SQS method for paramagnetic Fe. Next, we calculate energies of different magnetic distributions of Fe spins around impurity by changing the impurity positions inside the SQS used for the pure Fe. In our case, we used 50 positions of the impurity at different sites of the magnetic SQS. Finally, the obtained energies are averaged, giving the potential energy of the paramagnetic alloy ( $E(\text{Fe}_{1-c}X_c)$ ) with concentration  $c$  determined by the size of the SQS. Our goal is to approximate the potential energy of the paramagnetic alloy at high temperature  $T$ . Thus,  $\langle E(\text{Fe}_{1-c}X_c) \rangle$  should be defined as a thermal average over the “fast” magnetic degrees of freedom:

$$\langle E(\text{Fe}_{1-c}X_c) \rangle = -\frac{\partial \ln(Z)}{\partial \beta} = \sum_{\sigma} P_{\sigma} E_{\sigma}, \quad (1)$$

where  $Z = \sum_{\sigma} Z_{\sigma} = \sum_{\sigma} g_{\sigma} \exp\{-\beta E_{\sigma}\}$  is the canonical partition function,  $P_{\sigma}$  is the thermal probability of a particular MSM-SQS (magnetic) configuration  $\sigma$ , and  $\beta = \frac{1}{k_B T}$ , where  $k_B$  is the Boltzmann’s constant.  $E_{\sigma}$  and  $g_{\sigma}$  are the energy (per atom) and the multiplicity of each MSM-SQS configuration, respectively. In our calculations, all MSM samples are unique; thus,  $g_{\sigma} = 1$ .

The solution enthalpy is then defined as

$$\langle H_{\text{sol}} \rangle = \frac{\partial \Delta H_f}{\partial c}, \quad (2)$$

where

$$\Delta H_f = \langle E(\text{Fe}_{1-c}X_c) \rangle - (1-c)\langle E(\text{Fe}) \rangle - cE(X) \quad (3)$$

is the mixing enthalpy of the alloy,  $\langle E(\text{Fe}) \rangle = E_{\text{SQS}}(\text{Fe})$  is energy (per atom) of the magnetic SQS representing the paramagnetic Fe,  $\langle E(\text{Fe}_{1-c}X_c) \rangle$  is given by Eq. (1), and  $E(X)$  denotes the energy of the reference state for  $X$  ( $X = \text{C}, \text{N}, \text{V}, \text{Nb}$ ) impurity.

In the dilute limit, we find

$$\begin{aligned} \langle H_{\text{sol}} \rangle &= \left. \frac{\partial \langle E(\text{Fe}_{1-c}X_c) \rangle}{\partial c} \right|_{c \rightarrow 0} + \langle E(\text{Fe}) \rangle - E(X) \\ &= \frac{\langle E(\text{Fe}_{1-c}X_c) \rangle - \langle E(\text{Fe}) \rangle}{c} + \langle E(\text{Fe}) \rangle - E(X). \end{aligned} \quad (4)$$

For the supercell with a single interstitial impurity (C or N), Eq. (4) can be written as

$$\langle H_{\text{sol}} \rangle = (N+1)\langle E(\text{Fe}_{1-c}X_c) \rangle - N\langle E(\text{Fe}) \rangle - E(X), \quad (5)$$

where  $N$  is the number of atoms in the magnetic SQS representing pure Fe.

For substitutional impurities (V, Nb) we use

$$\langle H_{\text{sol}} \rangle = N\langle E(\text{Fe}_{1-c}X_c) \rangle - (N-1)\langle E(\text{Fe}) \rangle - E(X). \quad (6)$$

It is important to underline that the DLM picture neglects the magnetic short-range effects. Therefore, it is applicable at temperatures that are much higher than the magnetic transition temperature. While for the bcc Fe this may be a problem [42], the magnetic transition temperature for the fcc Fe is believed to be quite low, around room temperature. However, we aim to describe the impurities in high-temperature austenite, stable at  $T > 1183$  K [43]. Thus, the DLM picture should be adequate for our purpose. To further test the applicability of the latter, we compare the results of the solution enthalpies calculations using Eq. (1) for  $\langle E(\text{Fe}_{1-c}\text{X}_c) \rangle$  term with those where  $\langle E(\text{Fe}_{1-c}\text{X}_c) \rangle$  is obtained by an arithmetic average over MSM-SQS configurations. We find that for the two averaging methods the results differ by no more than 0.04 eV. This indicates that variations of energy between different magnetic configurations  $\sigma$  are much smaller than  $k_B T$ , and it justifies the use of the DLM picture, as well as the proposed MSM-SQS approach.

The effect of lattice vibrations is not treated explicitly in this paper. However, it is included, at least partly, via the thermal expansion of Fe lattice, as discussed in Sec. II.B. Also, in modeling the properties of pure  $\gamma$ -Fe using static calculations for the magnetic SQS, there is an unphysical effect of local relaxations between Fe atoms with different spin orientations, as discussed in detail in [41]. This error can be estimated from the energy difference  $\delta E$  between unrelaxed and statically relaxed SQS for pure (paramagnetic) fcc Fe. Our calculations give  $\delta E = 6.7$  meV/atom. The error due to the static approximation appears to be quite large. However, it should be to a large degree canceled in impurity solution enthalpy calculations, as the unphysical local lattice relaxations should be similar in Fe-X and Fe supercells. Indeed, recent calculations by Alling *et al.* [44] demonstrated the above error cancellation in calculations of the mixing enthalpy of (Cr-Al)N, and we do not expect that the situation should be drastically different in our case. Thus, the accuracy of our approach should be sufficient for the purpose of this paper.

### III. RESULTS

#### A. Influence of impurities on local geometry and magnetic properties of Fe host: Local and global effects

Though MSM-SQS configurations live time is  $\sim 1$  fs, it is still interesting to analyze our results for each magnetic sample. The lattice distortions around the impurity, in contrast to artificial local lattice relaxations due to the static approximation of the magnetic disorder discussed in Sec. II.C, is a physical effect, and they are highly important for the solution process. The local relaxations around impurity in Fe-X have been calculated as the average over a number of MSM realizations shifts of atomic positions  $\bar{R}^i$  from the ideal sites of the fcc crystal lattice for a specified coordination shell  $i$ :

$$\bar{R}^i = \frac{1}{n} \sum_{\sigma=1}^n \frac{1}{m_i} \sum_{i=1}^{m_i} \frac{(r(i) - r(0))}{r(0)}, \quad (7)$$

where  $m_i$  is the number of Fe atoms in the coordination shell  $i$ , the inner sum is taken over the coordination shell, the outer sum is taken over  $n$  MSM-SQS configurations  $\sigma$ , and  $r(i)$  and  $r(0)$  are the relaxed and the ideal Fe-X distances, respectively. In Eq. (7), we use arithmetic rather than the thermal average.

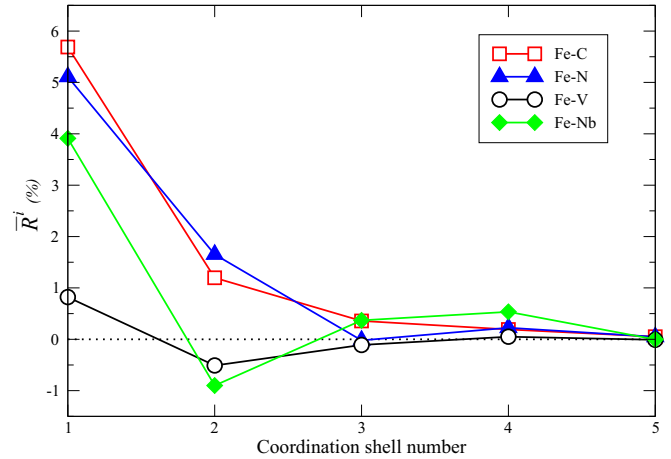


FIG. 2. (Color online) The average distortion  $\bar{R}^i$  (%) of host atoms in the first five coordination shells around C (red squares), N (blue triangles), V (black circles), and Nb (green diamonds) impurities in paramagnetic fcc Fe.

Our results are shown in Fig. 2. Analyzing the figure, one can see that the interstitial impurities, C and N, impose a tensile stresses on the surrounding lattice, while substitutional atoms, V and Nb, cause an oscillating stresses. Maximum relaxation for the first coordination sphere is found for carbon impurity ( $\sim 6\%$  relative to nondistorted Fe-C distance). Considering specific MSM-SQS configurations, we observe that in some cases Fe atoms surrounding impurity have large outward shifts (up to 9% for C), but sometimes there are small inward shifts (up to  $-2\%$  for V substitutional impurity). We conclude that for the considered impurities, the local lattice distortions are in general sufficiently high, and they should influence the calculated solution enthalpies.

Let us next analyze the magnetic properties of the impurities, as well as their influence on magnetic moments of the host atoms. Figure 3 shows local magnetic moments induced at the impurity atoms plotted as a function of the net magnetic moment of Fe atoms located in the first coordination shell of the impurity (Fe nearest-neighbor, or NN, cluster). We observe that for all systems, the magnitudes of the impurity magnetic moments are nearly proportional and their directions are antiparallel to the net magnetic moment of the Fe NN cluster, indicating that the impurity moments are induced by the host. Magnetic moments on the impurity atom vary from 0 to  $-0.15 \mu_B$  for carbon and from 0 to  $-0.09 \mu_B$  for nitrogen interstitial impurities. For the substitutional impurities, they are in the range 0 to  $-1.0 \mu_B$  and 0 to  $-0.4 \mu_B$  for V and Nb, respectively. Interestingly, the local lattice distortions do not seem to influence the general dependence of impurity magnetic moments on the net magnetic moment  $\Sigma \mu^{\text{Fe}}$  of Fe atoms located in the first coordination shell of the impurity. However, when relaxations are turned on, one clearly observes a clustering of the calculated results around certain values of  $\Sigma \mu^{\text{Fe}}$ . This indicates that the influence of the lattice distortions on the impurity magnetic moments comes mostly through their influence on the magnetism of the host Fe atoms.

In Fig. 4, we show mean magnetic moments at Fe atoms located near the impurity as a function of coordination shell  $i$  around the impurities. The averaging is carried out over the

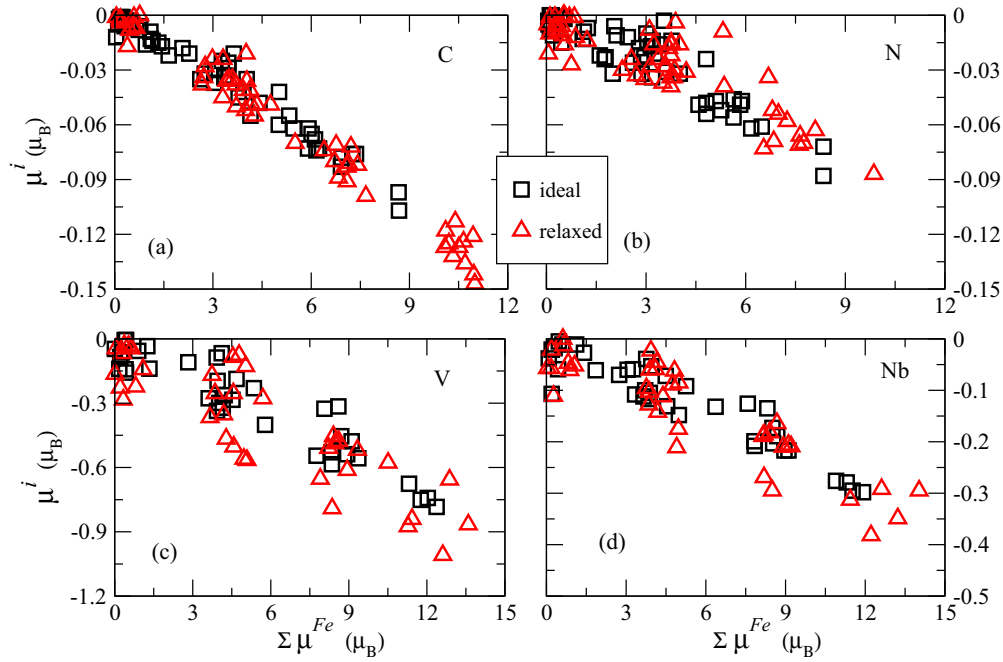


FIG. 3. (Color online) Local magnetic moments  $\mu_i$  (in  $\mu_B$ ) induced at the impurity atoms plotted as a function of the net magnetic moment  $\sum \mu^{Fe}$  (in  $\mu_B$ ) of Fe atoms located in the first coordination shell of (a) C, (b) N, (c) V, and (d) Nb impurities. Red triangles and black squares denote calculations with and without local lattice distortions around the impurities, respectively.

MSM-SQS realizations used in our simulations. The calculated mean magnetic moment for Fe atoms in pure paramagnetic fcc iron with experimental lattice parameter  $a = 3.64 \text{ \AA}$  is  $\sim 2.09 \mu_B$ . In all cases considered in this paper, the values of magnetic moments of the Fe atoms that are NN to the impurities are

reduced compared to those for the pure Fe matrix. The effect is especially strong for C and N impurities (Fig. 4(a) and 4(b)).

Similar behavior of magnetic moments as in Fig. 4 has been found at the grain boundaries in Ni by Vsianska and Sob [45] and in the neighborhood of isolated impurities in Ni by

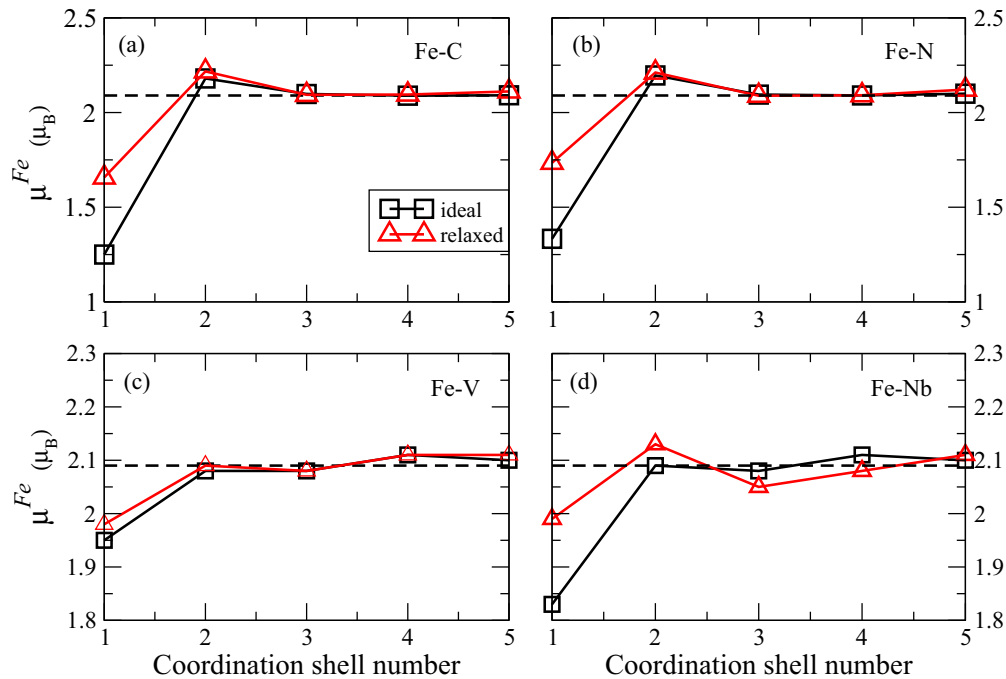


FIG. 4. (Color online) Mean absolute value of magnetic moments on Fe atoms as a function of coordination shell  $i$  around (a) C, (b) N, (c) V, and (d) Nb impurities. Averaging is done over the MSM-SQS realizations used in our simulations. Calculated mean magnetic moment for Fe atoms in pure paramagnetic fcc iron with experimental lattice parameter  $a = 3.64 \text{ \AA}$  is shown with horizontal dashed line. Red triangles and black squares denote calculations with and without local lattice distortions around the impurities, respectively.

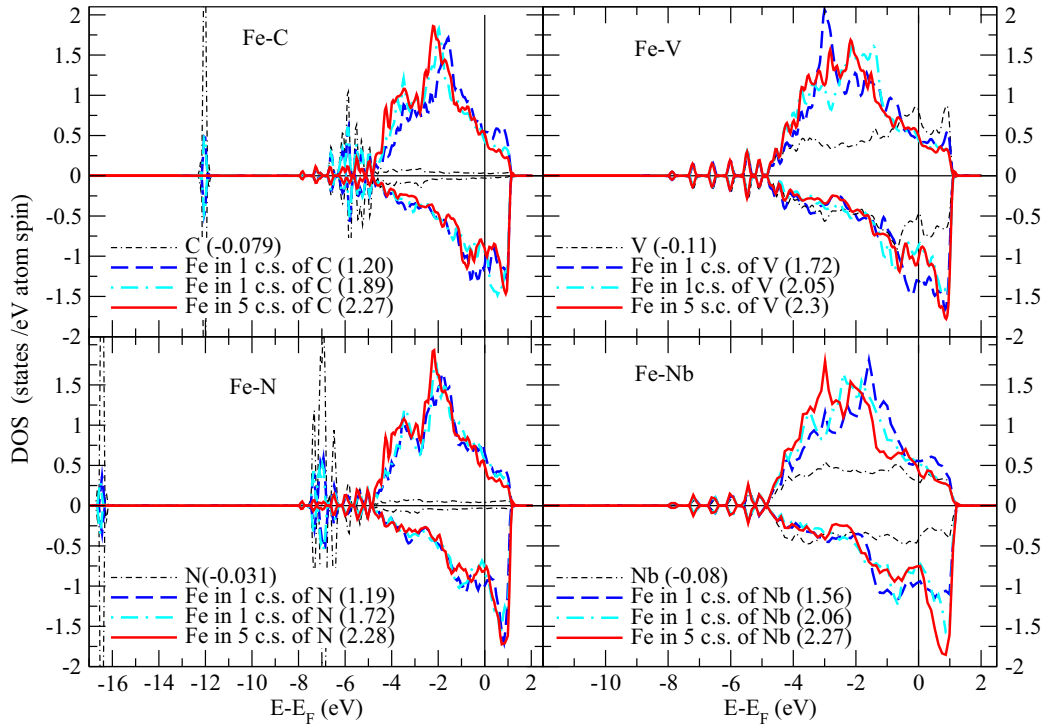


FIG. 5. (Color online) Calculated site-projected DOS of impurity atoms (C, N, V, and Nb; black dotted, two-dashed lines) and NN Fe atoms with different values of magnetic moments (Fe in 1 c.s.; blue dashed lines and cyan dashed-dotted lines). For comparison, the DOS of iron atoms located in the fifth coordination shell of the impurity (Fe in 5 c.s.; red lines) are also included. Values in parentheses correspond to the magnetic moments of the corresponding atoms.

Stefanou *et al.* [46]. According to those papers, the decrease of magnetic moments in the neighborhood of *sp* impurities is due to hybridization of the *sp* states of the impurity atom and *d* states of nickel atoms. Our calculations of density of states (DOS) of individual Fe and impurity atoms are consistent with results of Ref. [45]. Figure 5 shows site-projected DOS of impurity atoms (C, N, V, and Nb) and Fe atoms located in the first coordination shells of the impurity in relaxed supercells. Due to inhomogeneous strain around the impurity and the different magnetic environment, the magnetic moments of iron atoms differ even for the same coordination sphere, so in Fig. 5 we show the DOS of NN Fe atoms for two qualitatively different environments corresponding to the minimum and the maximum magnetic moments. Also the DOS of iron atoms located in the fifth coordination shell of the impurity are shown for comparison.

Analyzing results in Fig. 5, we see that for Fe atoms with a minimum magnetic moment occupying the first impurity sphere, there is the charge redistribution between up and down bands due to hybridization of *sp* (C, N) or *d* (V, Nb) electrons of the impurities with *d* electrons of Fe (Fig. 5). This leads to an increase of the DOS at the Fermi energy in the minority-spin subbands of iron and thus to lower magnetic moments. Interstitial impurities (C, N) have stronger influence on the DOS of the nearest Fe atoms than do substitution impurities (V, N); consequently, the decrease of the magnetic moment is more pronounced in Fe-C and Fe-N alloys. Also, in the relaxed state, reduction of the Fe magnetic moment around the impurity is less than in the case of the ideal, undistorted crystal lattice because the tensile stresses (Fig. 2) increase

Fe-X distances and reduce the hybridization between the orbitals of iron and the impurities. Note however that the analysis presented above should be taken with care. It is based on the electronic structure calculations at zero temperature, and therefore does not include temperature induced electronic and magnetic excitations. Here it is used primarily for the explanation of the trends seen in the behavior of magnetic moments on the host atoms around the impurity in Fig. 4, which are obtained within the same set of approximations.

We also see that the screening of the impurities is quite effective. The perturbation of the magnetic moments becomes very small already at the third shell of Fe atoms surrounding the impurity. The lattice distortions also decay by the third shell (Fig. 2). Interestingly, while the latter seem to have little effect in the induced magnetic moment of the impurity, they significantly reduce the perturbation of magnetic properties of the host, especially for NN Fe atoms (Fig. 4).

This effect can be understood if we consider the behavior of magnetic moments on Fe individual atoms. Figure 6 shows the dispersion of magnetic moments for all Fe atoms located in the first coordination shell of the impurities. The most remarkable features seen in Fig. 6 are that the dispersion is really large and that values of magnetic moments show much greater dispersion when they are calculated for ideal lattice positions than they do in the relaxed state. For V impurity, the lattice distortions are minimal, as is the dispersion of magnetic moments for NN Fe around the impurity, as well as the difference in the dispersion between the nondistorted and the relaxed states. The opposite is seen for interstitial impurities. The point is that local magnetic moments on Fe

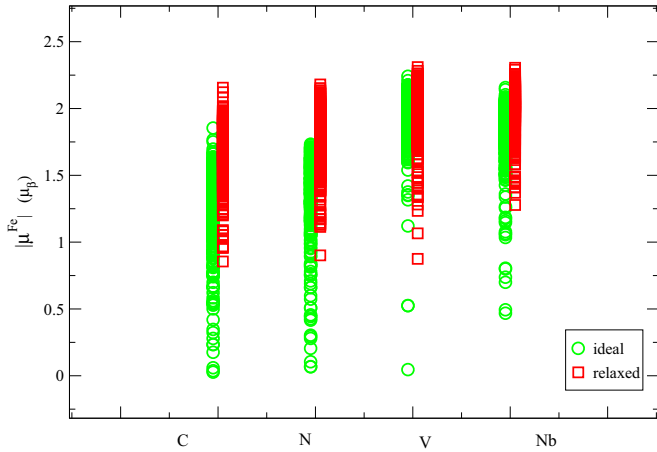


FIG. 6. (Color online) Calculated absolute values of magnetic moments of all Fe atoms located in the first coordination shell of C, N, V, and Nb impurities. Red squares and green circles denote calculations with and without local lattice distortions around the impurities, respectively.

are quite stable at the experimental lattice parameter. Indeed, even in the disordered state, their amplitude is above  $2 \mu_B$  for the pure Fe. Recent local density approximation +DMFT calculations by Igoshev *et al.* [5] showed that while at low temperature magnetism of fcc Fe is better described in terms of the itinerant picture, in the stability range of austenite it can be characterized by temperature-dependent effective local moments, which yield relatively narrow peaks in the real part of the local magnetic susceptibility as a function of frequency. Fixed spin moment calculations carried out for FM fcc Fe show that with increasing lattice parameter, a deep minimum is developing in the energy versus magnetic moment dependence [47], corresponding to increasing localization of the magnetic

moment. The situation should be similar in the DLM case. Therefore, substantial changes of Fe local magnetic moments have significant energy cost. Because the local distortions optimize the atomic positions to reduce the total energy, one achieves the most beneficial electronic structure and magnetization for each atom, bringing the magnetic moments closer to their values in pure Fe and reducing the heterogeneity of the magnetic structure. The magnetic moments at the impurities are obviously much less localized. They just follow the effective field induced by Fe NN moments.

Next, Fig. 7 shows the total energy calculated for all MSM supercells considered in this paper. The total energy is plotted versus the total magnetic moment of Fe atoms located in the first coordination sphere of impurity. First, for each specific magnetic configuration, we observe that results of calculations depended on the local magnetic environment of the impurity atom. This holds for the supercells with atoms at the ideal fcc positions, as well as for the calculations including local lattice relaxations. Second, we see that for the ideal supercells, the distribution of values of total energies versus the total magnetic moment of Fe NN cluster is more uniform, while in the relaxed state it is more discrete. A similar trend is observed for the distribution of magnetic moments on impurity atoms (Fig. 3), and it has been explained above. Our results therefore illustrate very high sensitivity of the energetic of the impure system on the local magnetic surrounding of the impurity. Thus, the effects of magnetic disorder must be treated explicitly in calculations of the solution enthalpy in magnetic materials above the magnetic transition temperature.

### B. Impurity solution enthalpies

Using the SQS-MSM described in Sec. II, we calculated the averaged impurity solution enthalpies for C, N, V, and

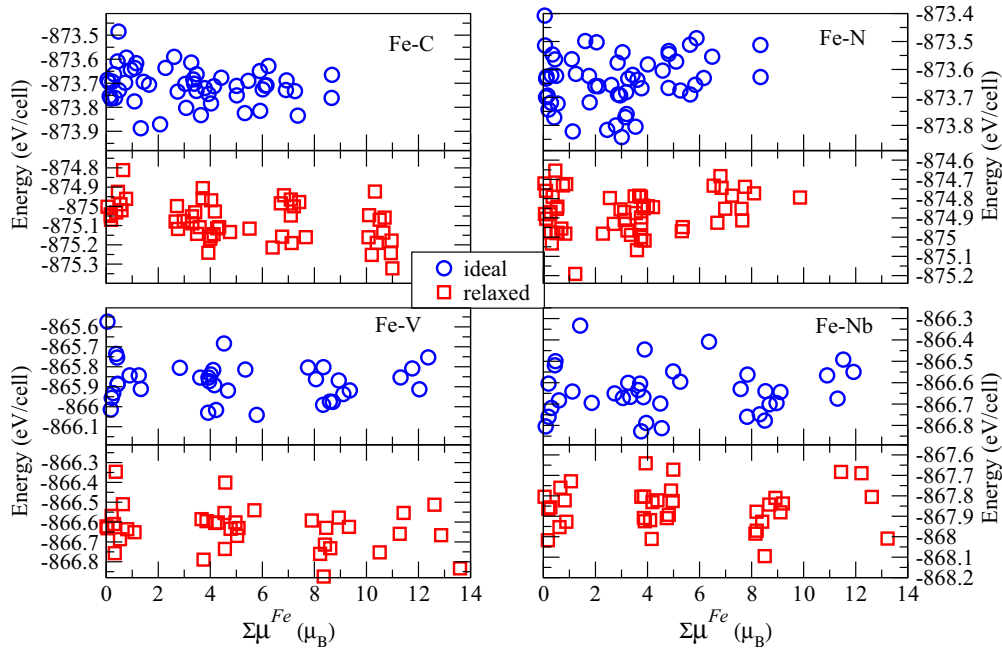


FIG. 7. (Color online) Calculated energies of MSM supercells with different impurity positions versus the total magnetic moment of Fe atoms located in the first coordination sphere of C, N, V, and Nb impurities. Red squares and blue circles correspond to calculations with and without local lattice distortions around the impurities, respectively.

TABLE I. Theoretical ( $\langle H_{\text{sol}} \rangle$ ) and experimental values of impurity solution enthalpy (in electron volts) of C, N, V, and Nb in paramagnetic fcc iron.

	Theory, MSM-SQS paramagnetic		Experiment
	Supercells with ideal fcc positions	Supercells with local lattice relaxations	
C	1.50	0.20	0.40 [24] 0.43 [48] 0.36 [49] 0.41 [50]
N	0.60	-0.39	-0.18 [51,52]
V	-0.20	-0.24	
Nb	1.2	0.36	

Nb in the paramagnetic fcc Fe. The results are presented in Table I. For the reference state energies in Eqs. (5) and (6), we used paramagnetic fcc Fe simulated within the magnetic SQS method and bcc crystals of V and Nb with theoretically calculated lattice parameters 3.03 and 3.30 Å, respectively, which turned out to coincide with experimental ones ( $a_{\text{exp}}^{\text{V}} = 3.02$  Å [53] and  $a_{\text{exp}}^{\text{Nb}} = 3.30$  Å [53]). An isolated dimer with the experimental bond length 1.1 Å was used as a reference state for N [54]. Because the van der Waals forces between graphite layers are not reproduced properly in the DFT-GGA calculations, for the reference state of C in Eq. (5) we used the hexagonal close-packed structure with the experimental lattice parameter  $a = 2.46$  Å and the lattice parameters  $c/a$  ratio 6.65 Å [55].

The results from Table I show that for impurities with strong local distortions of the host lattice in the first coordination shells (C, N, and Nb; Fig. 2), values of  $\langle H_{\text{sol}} \rangle$  calculated for MSM-SQS supercells with atoms at ideal fcc sites are strongly overestimated. They correspond to an endothermic process of the impurities dissolution for all three impurities. However, the calculations of the impurity solution enthalpies that include local lattice relaxations give lower values, which are significantly closer to the known experimental data. Moreover, the dissolution reaction of N is predicted to be exothermic, in agreement with experiment. For V impurity in fcc Fe, the influence of local lattice relaxations is smaller, in agreement with relatively small distortions introduced by V into the host lattice (Fig. 2).

Comparing our results with the experiment more carefully, data from Ref. [24] for the heat of the solution were obtained from carbon activity ( $a_{\text{C}}$ ) in Fe austenite in the temperature range  $T = 1056$ – $1120$  K and for the carbon fraction  $x_{\text{C}} = 2.5$ – $3.5$  at.%. In this interval of  $x_{\text{C}}$ , the solution enthalpy changes from 0.41 to 0.43 eV [24]. In that paper, empirical equations, representing  $H_{\text{sol}}$  and  $a_{\text{C}}$  as a function of  $T$  and  $x_{\text{C}}$ , were derived. Using these equations, we obtain the experimental value of  $H_{\text{sol}} = 0.38$  eV for carbon concentration  $x_{\text{C}} = 0.92$  at.% used in our calculations, which is somewhat closer to our theoretical value. The experimental value of the heat of solution for N in fcc Fe presented in Table I was obtained in Ref. [51] using experimental data of Ref. [52], where a thermogravimetric technique was used to determine

the solubility of nitrogen gas in solid iron. Unfortunately, we did not find any experimental data for dissolution enthalpies of substitutional impurities (V, Nb) in fcc Fe. Here, the literature information was limited to the values corresponding to dissolution of the carbides and nitrides and thermodynamic data on liquid and bcc phases of Fe. Thus, for the substitutional impurities, our values should be viewed as predictions.

To judge the quality of these predictions, we calculate the so-called solubility products of carbides VC, NbC and nitrides VN, NbN in austenite following the model proposed in Ref. [14]. A solubility product for a certain compound forming from a solution is the greatest value that the product of the concentrations of the constituents of the compound can take in that solution. Experimentally, solubility products appear over some temperature range to be rather well represented by straight lines in Arrhenius plots, and there are numerous estimations for this parameter, which is important for thermodynamic modeling, e.g., within the CALPHAD approach. Neglecting vibrational contributions to the free energy, and using Eqs. (19) and (21) from Ref. [14], we can write the Arrhenius temperature dependence of the solubility product for stoichiometric  $MeX$  ( $Me = \text{V, Nb}$  and  $X = \text{C, N}$ ) in fcc Fe as

$$\log_{10} K_s = A - \frac{B}{T} \approx \log_{10} \left( \frac{10^4 m_{Me} m_X}{m_{Fe}^2} \right) + \frac{[\Delta E_f(MeX) - \langle H_{\text{sol}} \rangle(Me) - \langle H_{\text{sol}} \rangle(X)]}{\ln 10 \cdot k_B \cdot T}, \quad (8)$$

where  $\Delta E_f(MeX)$  is the formation energy of  $MeX$  relative to the pure elements,  $\langle H_{\text{sol}} \rangle(Me)$  is the calculated solution enthalpy of V and Nb,  $\langle H_{\text{sol}} \rangle(X)$  is the calculated solution enthalpy of C or N, and  $m_{\text{Fe}, Me, X}$  is atomic mass of Fe or the impurities. For  $\Delta E_f(MeX)$ , we used standard enthalpy of formation:  $-1.05$  eV for VC [56],  $-2.2$  eV for VN [57],  $-1.4$  eV for NbC [56], and  $-2.4$  eV for NbN [56].

In Fig. 8, the calculated and experimental values of solubility product of  $MeX$  are displayed as a function of inverse temperature. One can see that the agreement between the calculated and the experimental values is quite good, especially for vanadium. Moreover, the calculated values of  $\log_{10} K_s$  show that in  $\gamma$ -Fe the nitrides are more stable than carbides, which coincides with experimental observations [12].

To illustrate the effect of the underlying magnetic state on the calculated impurity solution enthalpies, we carried out their calculations for FM fcc Fe. In principle, the magnetic ground state of the fcc Fe is believed to be a spin spiral, with a wave-vector  $q = [0, \xi_{XW}, 1]$ , where  $\xi_{XW} = 0.127$ . However, at the lattice parameter that corresponds to the high-temperature paramagnetic state, first-principles calculations show that there are nearly degenerate FM and double- and triple-layer antiferromagnetic solutions along [001] directions [64,65]. We therefore choose the former one, because it was the simplest and because our purpose was just to see how much the solution enthalpies change due to the magnetic order. The calculated values of  $\langle H_{\text{sol}} \rangle$  in FM fcc Fe for C, N, V, and Nb were found to be  $-0.10$ ,  $-0.72$ ,  $-0.40$ , and  $-0.04$  eV, respectively. A comparison of these values with  $\langle H_{\text{sol}} \rangle$  obtained for paramagnetic fcc Fe (Table I) showed that for all considered impurities, the values became significantly lower

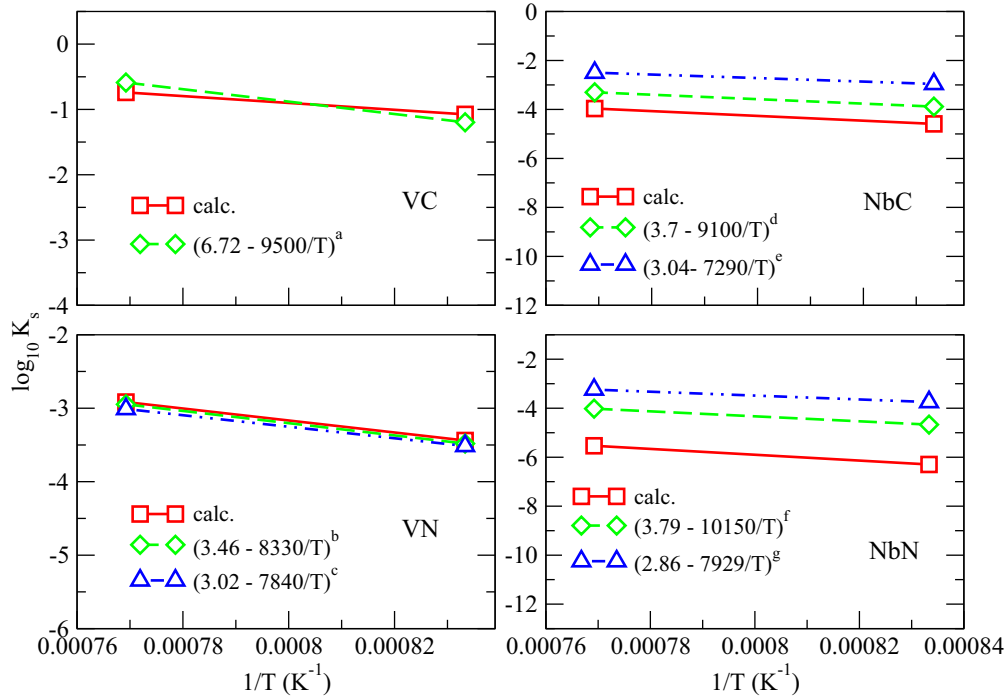


FIG. 8. (Color online) Solubility products of VC, VN, NbC, and NbN in paramagnetic  $\gamma$ -Fe. Experimental data are taken from <sup>a</sup>Ref. [58], <sup>b</sup>Ref. [12], <sup>c</sup>Ref. [59], <sup>d</sup>Ref. [60], <sup>e</sup>Ref. [61], <sup>f</sup>Ref. [62], and <sup>g</sup>Ref. [63].

and in worse agreement with the experiment. Thus, a proper treatment of the magnetic disorder was essential for theoretical determination of the impurity solution enthalpies.

The neglect of vibrational contribution in Eq. (8) may represent a serious approximation in the case of modeling the impurity solubility process [66]. Unfortunately, an evaluation of the relative importance of magnetic and vibrational disorder requires full-scale free-energy calculations for a magnetically disordered system, which cannot be carried out within the theoretical framework suggested here. Shulumba *et al.* [67] proposed a technique that allows one to achieve this goal and demonstrated that the magnetic disorder represents the major contribution, with respect to a vibrational one, for the description of phase stability of paramagnetic CrN. Good agreement of our calculations for the solubility product with the experiment may indicate that the situation is similar for the system considered in this paper.

In summary, we conclude that the proposed MSM-SQS approach gives reliable estimation of the impurity solution enthalpy in the paramagnetic state of fcc Fe. Possible sources of errors in calculations include limited supercell sizes, which do not capture long-range magnetic interactions in fcc Fe [26], the static description of the paramagnetic state [41], and an incomplete account of effects due to lattice vibrations, strong electron correlations, and longitudinal spin fluctuations.

#### IV. DISCUSSION

Let us discuss a possibility of induced magnetization around impurity in the paramagnetic state in the premartensitic temperature region. For instance, in our simulations of C impurity in paramagnetic fcc Fe, we sometimes observed a spin-flip (SF) transition, which occurs at Fe sites located in the

first coordination shell of the impurity atom. The SF transition is manifested by a change of orientation of a local magnetic moment during self-consistent iterations as compared to its original direction in the MSM-SQS supercell. This indicates that the carbon atom can induce the local magnetic polarization of the NN cluster in the paramagnetic fcc Fe. To further analyze this effect, we display in Fig. 9 the total magnetic moment on Fe sites, which are NNs to the impurity as a function of the total magnetic moment on the same Fe atoms in the pure matrix, that is, with the original orientations of disordered magnetic moments. The color map shows variations of  $H_{sol}$  for each MSM-SQS realization obtained in our calculations. Because average absolute values of magnetic moments of the Fe NN atoms are reduced for all impurities considered in this paper (Fig. 4), it could be expected that the final total magnetic moments of the Fe NN clusters also decrease, and calculated points in Fig. 9 should be located below the line  $y = x$ . However, in the case of the C impurity, one can see that a significant amount of calculated points ( $\sim 40\%$  of the total number of realization) show an increase of the magnetic moments of the Fe NN clusters, indicating an appearance of polarization around the impurity. These points are located in Fig. 9 above the line  $y = x$ . The reason for the increase is the observed SF transitions that occur at some Fe sites located in the first coordination shell of the carbon atom. Also, for Nb, V, and N, we found  $\sim 15\%$ ,  $8\%$ , and  $7\%$  of MSM-SQS realizations with the polarization, respectively. At the same time, there are some cases in which SFs lead to a decrease of the magnetic moments of the cluster around the impurities, i.e., to a depolarization. Almost all SF transitions are observed in calculations with fully relaxed atomic positions in the supercells. For supercells with atoms located at their ideal fcc positions, magnetic SFs around the impurities are either

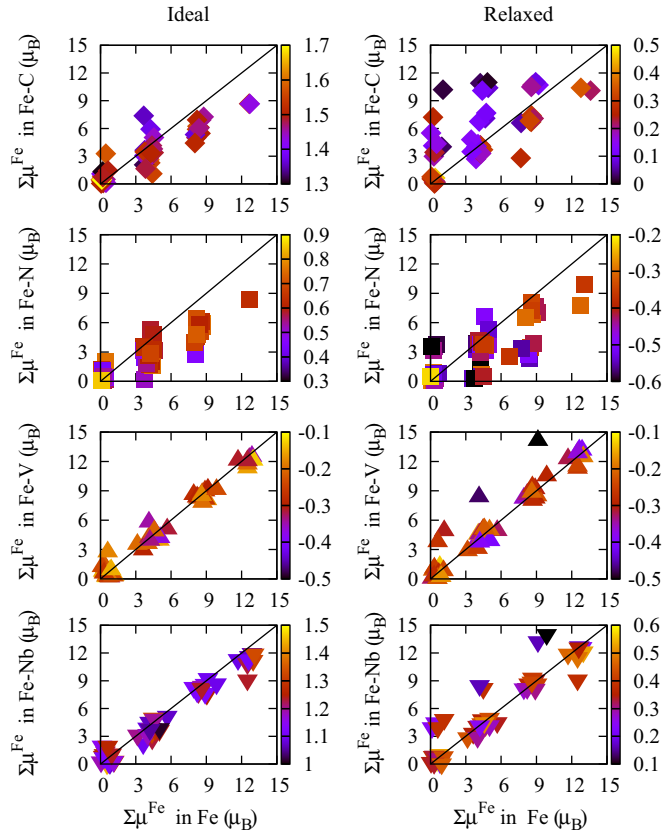


FIG. 9. (Color online) The total magnetic moment ( $\Sigma\mu^{\text{Fe}}$ , in  $\mu_B$ ) of Fe NN sites to the impurity as a function of the total magnetic moment of the same Fe atoms in the host SQS supercell. The color map shows variations of  $H_{\text{sol}}$  (in electron volts) for each MSM realization of the impure supercells. It smoothly ranges from black (minimum of  $H_{\text{sol}}$ , in electron volts), through violet and brown, to yellow (maximum of  $H_{\text{sol}}$ , in electron volts). The first and second columns correspond to calculations without and with local lattice distortions around the impurities, respectively.

absent (V) or appear seldom (2–4 MSM-SQS realizations for N, Nb, and C). These latter are supercells in which Fe atoms surrounding the impurity have large number of neighbors with parallel magnetic moments.

The appearance of the SF transitions in calculations with optimized atomic positions in the supercells can be explained as follows. It was established [26] that the NN pair exchange parameter  $J^{\text{Fe-Fe}}$  of the classical Heisenberg Hamiltonian  $H = -\sum J_{ij}e_i e_j$  in the FM state of  $\gamma$ -Fe at  $T = 0$  K is strongly volume dependent. Indeed,  $J$  was found to be negative for lattice parameter  $a$  between  $\sim 3.53$  and  $\sim 3.62$  Å and positive for  $a > 3.62$  Å. Similar behavior of the exchange parameters was observed in Ref. [23] from calculations based on spin spiral states of  $\gamma$ -Fe. Our calculations by the exact muffin-tin orbitals (EMTO) method combined with the CPA [68–72] using the DLM model for the paramagnetic state show that the tendency is similar even in paramagnetic pure  $\gamma$ -Fe:  $J^{\text{Fe-Fe}} < 0$  for  $a$  between 3.50 and 3.63 Å, and it sharply increases and becomes positive for larger values of lattice parameters (Fig. 10). The experimental value of the lattice parameter of pure fcc Fe (3.64 Å) is located in the transition

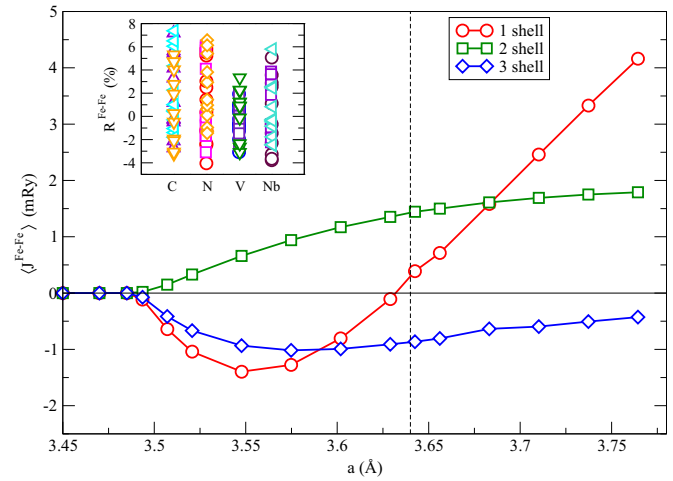


FIG. 10. (Color online) Calculated average pair exchange parameter  $\langle J^{\text{Fe-Fe}} \rangle$  in fcc Fe in a static DLM state for first, second, and third coordination shells as a function of the lattice parameter. The EMTO-CPA method has been employed for the calculations. The inset shows the relative atomic displacements  $R^{\text{Fe-Fe}}$  (%) between the iron atoms Fe-Fe within the Fe NN cluster for some Fe-X realizations.

region, with nearly zero value of the exchange integral for the first coordination shell (Fig. 10).

As has been shown above (Fig. 2), the average relaxations of atomic positions in Fe-X on the first coordination shell are tensile for all impurities. At the same time, changes in the distances between the iron atoms ( $R^{\text{Fe-Fe}}$ ) within each Fe NN cluster are not homogeneous, with either large outward or inward atomic displacements (inset of Fig. 10).

It can be assumed that due to strong dependence of  $J^{\text{Fe-Fe}}$  on interatomic distance, the sign of the exchange parameter can change for such a distorted pair of Fe atoms. In the case of large outward relaxations, the exchange interactions between neighboring atoms of iron should be shifted towards positive values, which could lead to a formation of partially or completely FM Fe clusters around the impurity via SFs. However, inward relaxations can shift the exchange interactions into the antiferromagnetic region. In this case, a depolarization of the Fe NN cluster should occur.

In our calculations, the maximal change of the local magnetic structure due to the polarization effect described above is found for the carbon impurity, for which outward Fe-Fe atomic displacements are also maximal. In addition, we can trace a direct link between the occurrence of polarization in Fe-C and a decrease of solution enthalpy  $H_{\text{sol}}^{\sigma}$  (Fe-C). If we exclude from the summation in Eq. (4) the configurations with SF, the solution enthalpy of carbon becomes equal to 0.27 eV; i.e., it increases by almost 35%. Here, the polarization in its static form is unlikely to be seen in the high-temperature paramagnetic state of fcc Fe-X alloys. But in the temperature range of overcooled austenite, one should expect the formation of a local Fe cluster around carbon with predominantly FM coupling. In this case, the polarization effect may cause a change in the interatomic bonding between C and Fe atoms, which in turn may lead to a change of macroscopic properties, for example, thermodynamic activity of carbon.

TABLE II. Solution enthalpies  $H_{\text{sol}}^\sigma$  for one Fe- $X$  configuration calculated either at fixed volume ( $V$ ) or at fixed pressure ( $P$ ) of both Fe- $X$  and Fe supercells in relaxed states.

	$H_{\text{sol}}^\sigma$ , eV		
	$P_1(\text{Fe-}X) = P_1(\text{Fe})$ $V_1(\text{Fe-}X) \neq V_1(\text{Fe})$	$P_2(\text{Fe}) = P_2(\text{Fe-}X)$ $V_2(\text{Fe-}X) \neq V_2(\text{Fe})$	$V_1(\text{Fe-}X) = V_2(\text{Fe})$ $P(\text{Fe-}X) \neq P(\text{Fe})$
Fe-C $P_1 = 128.2$ kbar, $P_2 = 132.4$ kbar	0.27	0.25	-0.33
Fe-N $P_1 = 127.7$ kbar, $P_2 = 132.4$ kbar	-0.42	-0.44	-1.08
Fe-V $P_1 = 132.2$ kbar, $P_2 = 132.4$ kbar	-0.20	-0.24	-0.26
Fe-Nb $P_1 = 126.6$ kbar, $P_2 = 132.4$ kbar	0.43	0.42	-0.38

V. SUMMARY

The solution enthalpy of substitutional (V, Nb) and interstitial (C, N) impurities in paramagnetic fcc Fe (austenite) has been investigated by means of first-principles electronic structure calculations using (PAW-GGA) VASP. The paramagnetic state was modeled by a supercell realization of the DLM model in the framework of MSM combined with the SQS approach. In the proposed technique, the magnetic SQS supercell was created for the host, fcc Fe, and then calculations for impurities located at different positions of the supercell were performed, followed by the averaging of the results as supposed by the MSM. We show that the SQS-MSM approach gives estimations of solution enthalpies with accuracy similar to what is expected for first-principles calculations in magnetically ordered and nonmagnetic materials (see, e.g., [73]), although, as the calculated and measured solution enthalpies are small, relative deviations between them are significant in cases of C and N. Nevertheless, solubility products for corresponding carbides and nitrides in the paramagnetic state calculated with the proposed approach are in agreement with available experimental data. We found that all impurities can induce a local magnetic polarization of Fe atoms neighboring the impurity by the SF transitions. Induced magnetization is especially pronounced for a carbon atom and can lead to a change of the magnetic structure in overcooled austenite. In addition, for carbon, we have established a correlation between the occurrence of polarization and the decrease of solution enthalpy.

ACKNOWLEDGMENTS

We are grateful to Prof. A. V. Ruban and Prof. P. A. Korzhavyi for useful discussions. This paper was supported by the Russian Federation Ministry for Science and Education (Grant No. 14.Y26.31.0005). Support provided by the Swedish Foundation for Strategic Research, program Succesful Research Leader Grant No. 744 10-0026 is gratefully acknowledged. The Russian Foundation for Basic Researches (Grant

No. 13-02-00-606a) is acknowledged for financial support. Calculations were performed at the Joint Supercomputer Center of the Russian Academy of Sciences (Moscow) and the Swedish National Infrastructure for Computing at the National Supercomputer Centre in Linköping, Sweden.

APPENDIX

A. Solution enthalpy for one configuration:  $V = \text{const}$  and  $P = \text{const}$

In this paper, the solution enthalpy calculations were carried out at the experimental lattice parameters and constant theoretical pressure. To demonstrate the specific features of carrying out impurity calculations at the experimental high-temperature lattice parameter, which differ significantly from the one corresponding to the zero-temperature energy minimum, we show in Table II the solution enthalpies  $H_{\text{sol}}^\sigma$  for one specific magnetic configuration in each Fe- $X$  system calculated either at fixed volume ( $V$ ) or at fixed zero-temperature pressure ( $P$ ) for both Fe- $X$  and pure Fe SQS supercells, that is, for the  $V(\text{Fe-}X) = V(\text{Fe})$  and the  $P(\text{Fe-}X) = P(\text{Fe})$  cases, respectively. Atom positions in the supercells are optimized by allowing for the local lattice relaxations. Also, for the fixed zero-temperature pressure calculations, we check whether the solution enthalpies change depending on small variations of pressure. Here,  $P_1$  corresponds to the zero-temperature pressure of the Fe- $X$  supercell with the experimental volume and  $P_2$  corresponds to the zero-temperature pressure of the pure Fe magnetic SQS supercell with the same volume.

We see that for a calculation at the fixed volume, the solution enthalpy is much lower for all impurities except for vanadium. At the same time, a slight shift of the pressure has little effect on  $H_{\text{sol}}^\sigma$ . For C and N calculations, values of  $H_{\text{sol}}^\sigma$  at a fixed volume do not agree with available experimental data (Table I). For the Fe-V case, we find that pressure in  $V = \text{const}$  and  $P = \text{const}$  simulations are almost equal. Thus, the calculations of solution enthalpy give comparable results.

[1] T. Moriya, *Spin Fluctuations in Itinerant Electron Magnetism* (Springer, Berlin, Germany, 1985).

[2] A. Georges, G. Kotliar, W. Krauth, and M. Rozenberg, *Rev. Mod. Phys.* **68**, 13 (1996).

- [3] A. I. Lichtenstein, M. I. Katsnelson, and G. Kotliar, *Phys. Rev. Lett.* **87**, 067205 (2001).
- [4] L. V. Pourovskii, T. Miyake, S. I. Simak, A. V. Ruban, L. Dubrovinsky, and I. A. Abrikosov, *Phys. Rev. B* **87**, 115130 (2013).
- [5] P. A. Igoshev, A. V. Efremov, A. I. Poteryaev, A. A. Katanin, and V. I. Anisimov, *Phys. Rev. B* **88**, 155120 (2013).
- [6] I. Leonov, A. I. Poteryaev, V. I. Anisimov, and D. Vollhardt, *Phys. Rev. Lett.* **106**, 106405 (2011).
- [7] K. Glazyrin, L. V. Pourovskii, L. Dubrovinsky, O. Narygina, C. McCammon, B. Hewener, V. Schünemann, J. Wolny, K. Muffler, A. I. Chumakov, W. Crichton, M. Hanfland, V. Prakapenka, F. Tasnádi, M. Ekholm, M. Aichhorn, V. Vildosola, A. V. Ruban, M. I. Katsnelson, and I. A. Abrikosov, *Phys. Rev. Lett.* **110**, 117206 (2013).
- [8] J. Hubbard, *Phys. Rev. B* **19**, 2626 (1979); **20**, 4584 (1979); **23**, 5974 (1981).
- [9] H. Hasegawa, *J. Phys. Soc. Jpn.* **46**, 1504 (1979); **49**, 178 (1980).
- [10] B. L. Gyorffy, A. J. Pindor, J. Staunton, G. M. Stocks, and H. Winter, *J. Phys. F* **15**, 1337 (1985).
- [11] B. Alling, T. Marten, and I. A. Abrikosov, *Phys. Rev. B* **82**, 184430 (2010).
- [12] T. Gladman, *The Physical Metallurgy of Microalloyed Steels* (The Institute of Metals, Institute of Materials Press, London, 1997).
- [13] R. Lagneborg, T. Siwecki, S. Zajac, and B. Hutchinson, *Scand. J. Metall.* **28**, 186 (1999).
- [14] T. Klimko and M. H. F. Sluiter, *J. Mater. Sci.* **47**, 7601 (2012).
- [15] W. F. Smith and J. Hashemi, *Foundations of Materials Science and Engineering*, 4th ed. (McGraw-Hill, Dallas, TX, 2005).
- [16] D. W. Boukhvalov, Yu. N. Gornostyrev, M. I. Katsnelson, and A. I. Lichtenstein, *Phys. Rev. Lett.* **99**, 247205 (2007).
- [17] D. E. Jiang and E. A. Carter, *Phys. Rev. B* **67**, 214103 (2003).
- [18] Y. Tsunoda, *J. Phys.: Condens. Matter* **1**, 10427 (1989).
- [19] Y. Tsunoda, Y. Nishioka, and R. M. Nicklow, *J. Magn. Magn. Mater.* **128**, 133 (1993).
- [20] O. N. Mryasov, A. I. Lichtenstein, L. M. Sandratskii, and V. A. Gubanov, *J. Phys.: Condens. Matter* **3**, 7683 (1991).
- [21] M. Körling and J. Ergon, *Phys. Rev. B* **54**, R8293 (1996).
- [22] S. Shallcross, A. E. Kissavos, S. Sharma, and V. Meded, *Phys. Rev. B* **73**, 104443 (2006).
- [23] S. V. Okatov, Yu. N. Gornostyrev, A. I. Lichtenstein, and M. I. Katsnelson, *Phys. Rev. B* **84**, 214422 (2011).
- [24] J. A. Lobo and G. H. Geiger, *Metall. Mater. Trans. A* **7**, 1359 (1976).
- [25] R. P. Smith, *Trans. Metallurg. Soc. AIME* **230**, 476 (1964).
- [26] A. V. Ruban, M. I. Katsnelson, W. Olovsson, S. I. Simak, and I. A. Abrikosov, *Phys. Rev. B* **71**, 054402 (2005).
- [27] A. Reyes-Huamantínco, P. Puschnig, C. Ambrosch-Draxl, O. E. Peil, and A. V. Ruban, *Phys. Rev. B* **86**, 060201 (2012).
- [28] G. Kresse and J. Furthmüller, *Comput. Mater. Sci.* **6**, 15 (1996); *Phys. Rev. B* **54**, 11169 (1996).
- [29] G. Kresse and J. Joubert, *Phys. Rev. B* **59**, 1758 (1999).
- [30] P. E. Blöchl, *Phys. Rev. B* **50**, 17953 (1994).
- [31] J. P. Perdew, K. Burke, and M. Ernzerhof, *Phys. Rev. Lett.* **77**, 3865 (1996).
- [32] H. Hellmann, *Einführung in die Quantenchemie* (Deuticke, Leipzig, Germany, 1937).
- [33] R. P. Feynman, *Phys. Rev.* **56**, 340 (1939).
- [34] M. Methfessel and A. T. Paxton, *Phys. Rev. B* **40**, 3616 (1989).
- [35] H. J. Monkhorst and J. D. Pack, *Phys. Rev. B* **13**, 5188 (1976).
- [36] M. Onink, C. M. Brakman, F. D. Tichelaar, E. M. Mittemeijer, S. van der Zwaag, J. H. Root, and N. B. Konyer, *Scripta Metall. Mater.* **29**, 1011 (1993).
- [37] S.-J. Lee, M. T. Lusk, and Y.-K. Lee, *Acta Mater.* **55**, 875 (2007).
- [38] Landolt-Börnstein, in *Magnetic Properties of Metals: 3d, 4d and 5d Elements, Alloys and Compounds, New Series, Group III*, edited by K. Kanematsu, S. Misawa, M. Shiga, H. Wada, and H. P. J. Wijn, (Springer-Verlag, Berlin, 1997), Vol. 32A.
- [39] A. Filippetti, W. E. Pickett, and B. M. Klein, *Phys. Rev. B* **59**, 7043 (1999).
- [40] A. Zunger, S.-H. Wei, L. G. Ferreira, and J. E. Bernard, *Phys. Rev. Lett.* **65**, 353 (1990).
- [41] P. Steneteg, B. Alling, and I. A. Abrikosov, *Phys. Rev. B* **85**, 144404 (2012).
- [42] A. V. Ruban and V. I. Razumovskiy, *Phys. Rev. B* **85**, 174407 (2012).
- [43] R. Abbaschian, L. Abbaschian, and R. E. Reed-Hill, *Physical Metallurgy Principles*, 4th ed. (Cengage Learning, Stamford, USA, 2009).
- [44] B. Alling, L. Hultberg, L. Hultman, and I. Abrikosov, *Appl. Phys. Lett.* **102**, 031910 (2013).
- [45] M. Vsianska and M. Sob, *Progr. Mat. Sci.* **56**, 817 (2011).
- [46] N. Stefanou, A. Oswald, R. Zeller, and P. H. Dederichs, *Phys. Rev. B* **35**, 6911 (1987).
- [47] I. A. Abrikosov, O. Eriksson, P. Söderlind, H. L. Skriver, and B. Johansson, *Phys. Rev. B* **51**, 1058 (1995).
- [48] R. P. Smith, *J. Amer. Chem. Soc.* **68**, 1163 (1946).
- [49] J. A. Slane, C. Wolverton, and C. R. Gibala, *Metall. Mater. Trans. A* **35**, 2239 (2004).
- [50] T. Ellis, I. M. Davidson, and C. Bodsworth, *J. Iron Steel Inst.* **201**, 582 (1963).
- [51] D. Bouchard and J. S. Kirkaldy, *J. Alloys Compd.* **283**, 311 (1999).
- [52] M. Hillert and M. Jarl, *Met. Trans. A* **6**, 553 (1975).
- [53] R. Ferro and A. Saccone, *Intermetallic Chemistry* (Elsevier, Amsterdam, the Netherlands, 2008), Vol. 13, pp. 407.
- [54] M. Grunze, M. Golze, W. Hirschwald, H.-J. Freund, H. Pulm, U. Seip, M. C. Tsai, G. Ertl, and J. Küppers, *Phys. Rev. Lett.* **53**, 850 (1984).
- [55] A. Ludstch, *Acta Crystallogr. A Cryst. Phys. Diffr. Theor. Gen. Crystallogr.* **28**, 59 (1972).
- [56] C. Smithells, *Smithells Metals Reference Book*, 6th ed. (Butterworth, London, UK, 1983), p. 22.
- [57] A. D. Mah, *U.S. Bur. Mines. No.* 6177 (1963).
- [58] K. Narita, *Trans. Iron Steel Inst. Jpn.* **15**, 145 (1975).
- [59] A. T. Davenport, L. C. Brossard, and R. E. Milner, *J. Metals* **27**, 21 (1975).
- [60] R. P. Smith, *Trans. Metallurg. Soc. AIME* **236**, 1224 (1966).
- [61] L. Meyer, *Z. Metallkd.* **58**, 334 (1967).
- [62] T. Mori, M. Tokizane, K. Yamaguchi, E. Sumani, and Y. Nakazima, *Tetsu-to-Hagane* **54**, 763 (1968).
- [63] R. C. Sharma, V. K. Lakshmanan, and J. S. Kirkaldy, *Met. Trans. A* **15**, 545 (1984).
- [64] P. James, O. Eriksson, B. Johansson, and I. A. Abrikosov, *Phys. Rev. B* **59**, 419 (1999).
- [65] I. A. Abrikosov, A. E. Kissavos, F. Liot, B. Alling, S. I. Simak, O. Peil, and A. V. Ruban, *Phys. Rev. B* **76**, 014434 (2007).
- [66] V. Ozolins and M. Asta, *Phys. Rev. Lett.* **86**, 448 (2001).

- [67] N. Shulumba, B. Alling, O. Hellman, E. Mozafari, P. Steneteg, M. Odén, and I. A. Abrikosov, *Phys. Rev. B* **89**, 174108 (2014).
- [68] L. Vitos, *Phys. Rev. B* **64**, 014107 (2001).
- [69] L. Vitos, I. A. Abrikosov, and B. Johansson, *Phys. Rev. Lett.* **87**, 156401 (2001).
- [70] P. Soven, *Phys. Rev.* **156**, 809 (1967).
- [71] B. L. Gyorffy, *Phys. Rev. B* **5**, 2382 (1972).
- [72] J. S. Faulkner, *Prog. Mater. Sci.* **27**, 1 (1982).
- [73] B. Drittler, M. Weinert, R. Zeller, and P. H. Dederichs, *Phys. Rev. B* **39**, 930 (1989).